POTSDAM-INSTITUT FÜR
KLIMAFOLGENFORSCHUNG

AGU PUBLICATIONS

Geophysical Research Letters

RESEARCH LETTER
10.1002/2016GL069700

Key Points:
- Large ensembles of stratospheric ozone projections and dates of return of ozone to 1960 levels are reported for the first time
- Analysis shows strong dependence of the spread in dates of return on latitude and greenhouse gas emissions scenarios

Supporting Information:
- Supporting Information S1

Correspondence to:
A. H. Södergren,
helena@bodekerscientific.com

Citation:
Södergren, A. H., G. E. Bodeker, S. Kremser, M. Meinshausen, and A. J. McDonald (2016), A probabilistic study of the return of stratospheric ozone to 1960 levels, *Geophys. Res. Lett.*, *43*, 9289–9297, doi:10.1002/2016GL069700.

Received 25 MAY 2016
Accepted 5 AUG 2016
Accepted article online 9 AUG 2016
Published online 5 SEP 2016

A probabilistic study of the return of stratospheric ozone to 1960 levels

A. Helena Södergren[1,2], Gregory E. Bodeker[1], Stefanie Kremser[1], Malte Meinshausen[3,4], and Adrian J. McDonald[2]

[1]Bodeker Scientific, Alexandra, New Zealand, [2]Department of Physics and Astronomy, University of Canterbury, Christchurch, New Zealand, [3]School of Earth Sciences, University of Melbourne, Parkville, Victoria, Australia, [4]Earth System Analysis, Potsdam Institute for Climate Impact Research, Potsdam, Germany

Abstract Anthropogenic emissions of greenhouse gases and ozone-depleting substances are expected to continue to affect concentrations of ozone in the stratosphere through the 21st century. While a range of estimates for when stratospheric ozone is expected to return to unperturbed levels is available in the literature, quantification of the spread in results is sparse. Here we present the first probabilistic study of latitudinally resolved years of return of stratospheric ozone to 1960 levels. Results from our 180-member ensemble, simulated with a newly developed simple climate model, suggest that the spread in return years of ozone is largest around 40°N/S and in the southern high latitudes and decreases with increasing greenhouse gas emissions. The spread in projections of ozone is larger for higher greenhouse gas scenarios and is larger in the polar regions than in the midlatitudes, while the spread in ozone radiative forcing is smallest in the polar regions.

1. Introduction

Chemistry climate models (CCMs) are the tools most commonly used to project the future evolution of the ozone layer [*World Meteorological Organization* (*WMO*), 2014]. Uncertainties in projections of ozone arise due to a wide range of plausible future greenhouse gas (GHG) and ozone-depleting substance (ODS) emissions scenarios, as well as differences between models [*Eyring et al*., 2007, 2010a, 2010b; *Charlton-Perez et al*., 2010; *Nowack et al*., 2015]. The complexity and resultant high computational costs of CCM simulations, however, preclude a thorough exploration of the uncertainty space.

Since the 1970s, anthropogenic emissions of ODSs have led to a global depletion of stratospheric ozone, most severe over Antarctica in late winter and spring. The Montreal Protocol, with its amendments and adjustments, has led to observed decreases in tropospheric concentrations of controlled ODSs which are expected to return to 1960 levels around the end of the 21st century [*World Meteorological Organization (WMO)*, 2007]. The decline of ozone outside the polar regions has been reported to have ceased in the late 1990s, meeting the criterion for the first stage of ozone recovery [*WMO*, 2007].

As atmospheric concentrations of ODSs decline, other factors, such as changes in the climate of the stratosphere due to ongoing emissions of GHGs, will increasingly influence stratospheric ozone [*WMO*, 2014; *Eyring et al*., 2010b; *Bekki et al*., 2013; *Gauss et al*., 2006; *Shepherd and Jonsson*, 2008]. Increasing concentrations of GHGs alter the abundances of stratospheric ozone through decreases in stratospheric temperatures which in turn affect temperature-dependent chemical reactions (e.g., slowing of the $O_3 + O \rightarrow O_2$ reaction), through changes in hydrogen and nitrogen oxide chemistry and through GHG-induced changes in transport [*Jonsson et al*., 2004; *Eyring et al*., 2007]. For example, GHG-induced radiative warming of the troposphere affects transport pathways of ozone, ozone precursors (nitrogen oxides, carbon monoxide, and volatile organic compounds), and ODSs to the stratosphere. One such transport pathway is the Brewer Dobson circulation (BDC) [*Butchart*, 2014] which globally redistributes ozone produced primarily in the tropical upper stratosphere. Changes in the BDC also affect the rate at which ODS photolyze.

Simple climate models (SCMs) can be used as fast emulators of complex atmosphere-ocean general circulation models (AOGCMs) [*Randall et al*., 2007]. While a SCM cannot replace more sophisticated AOGCMs, it offers a complementary research tool that can synthesize and consistently integrate a range of uncertainties resulting from our imperfect knowledge of the climate system and of future emissions. To date, and to our

knowledge, no SCM has incorporated an interactive stratosphere which has precluded the use of SCMs in diagnosing uncertainties in projections of stratospheric ozone.

Here we present a SCM that has been extended to include an interactive stratosphere and its application to simulating the evolution of the ozone layer through the 21st century. To our knowledge, this is the first probabilistic study of the years of return of stratospheric column ozone (SCO) to 1960 levels.

2. Methods

A new interactive SCM has been developed as an extension to the Model for Assessment of Greenhouse-gas Induced Climate Change (MAGICC) [*Meinshausen et al*., 2011a, 2011b] SCM. In this new version of MAGICC, the radiative forcing (RF; downward minus upward flux at the tropopause) from stratospheric ozone couples simulated ozone changes to the climate system in the model. Resultant changes to surface temperatures, and thereby other components of MAGICC sensitive to surface temperature, affect stratospheric carbon dioxide (CO_2) concentrations and hence stratospheric temperatures which affect ozone chemistry. This two-way coupling is important for simulating SCO.

MAGICC generates an estimate of equivalent effective stratospheric chlorine (EESC, derived from chlorine and bromine) [*Daniel et al*., 1999; *Newman et al*., 2007] and CO_2 concentrations at the end of each model year. The estimated CO_2 and EESC provide the inputs needed to simulate SCO and RF within MAGICC. A pattern scaling technique, previously applied to surface climate variables [*Kremser et al*., 2014; *Mitchell*, 2003], was used to statistically model the dependence of (1) SCO on EESC and CO_2, (2) the vertically weighted SCO (wSCO) on EESC and CO_2, and (3) stratospheric ozone RF on wSCO.

SCO is modeled since this is of direct interest to policy makers (in terms of dates of return of ozone to unperturbed levels). EESC is a measure of the net effect of chlorine and bromine on ozone and is therefore included as a predictor in the ozone regression models (section 2.1). CO_2 is also included as a predictor since it affects stratospheric temperatures which in turn impact ozone chemistry.

RF depends on the altitude at which the change in ozone occurs [*Forster and Shine*, 1997; *Lacis*, 1990], and to capture this, the ozone profile that is used to calculate SCO is weighted so that the ozone near the tropopause has a greater influence on the RF. The simulated wSCO is used in a second regression model (section 2.2).

Ozone RF is simulated in MAGICC so that modeled changes in ozone modulate the total RF thereby coupling stratospheric ozone changes to the climate system. A third regression model was trained on the vertically weighted ozone and its corresponding RF (section 2.3).

2.1. Statistical Modeling of SCO

The regression model used to capture the functional dependence of zonal mean SCO anomalies on global EESC and CO_2 anomalies is of the form

$$SCO_i' = \alpha_i EESC' + \beta_i CO_2' + \varepsilon \tag{1}$$

The primes in equation (1) denote anomalies with respect to 1960 levels, and the coefficients α, β, and ε are obtained from fitting equation (1) to CCM output for each latitude zone *i*. Daily zonal mean SCO′ and EESC′, simulated by the European Centre/Hamburg/Modular Earth Submodel System Atmospheric Chemistry (EMAC) [*Jöckel et al*., 2006] CCM, and CO_2 anomalies following the RCP8.5 emissions scenario, were used to derive the fit coefficients. Fit coefficients are derived across the 64 latitude zones represented in EMAC.

To capture the seasonal dependence of SCO′ on EESC′ and CO_2′, the fit coefficients in equation (1) are expanded in a Fourier series:

$$\alpha(t) = \alpha_0 + \sum_{k=1}^{M}\left[\alpha_{2k-1}\sin\left(2\pi k\frac{t}{365}\right) + \alpha_{2k}\cos\left(2\pi k\frac{t}{365}\right)\right] \tag{2}$$

where *t* is the day of the year and *M* is the number of Fourier pairs to which the fit coefficient is expanded. The value of *M* can be set depending on the seasonal structure expected in the fit coefficients. For the analysis presented here, *M* in equation (2) was set to 4 for ε in equation (1) and 2 for α and β.

In our model, the effects of GHGs on the abundances of polar stratospheric clouds (PSCs), by virtue of their cooling effect on the stratosphere, are not directly accounted for. Because PSCs are essential for the polar heterogeneous chemistry that causes severe ozone depletion [*Hamill et al*., 1986; *Huck et al*., 2013], increases in GHG concentrations increase the ubiquity of PSCs and reduce ozone. Our methodology considers only the positive effects of GHG-induced stratospheric cooling on ozone Chapman chemistry. That said, the effects of PSCs on polar ozone are captured in our regression model of SCO in the form of elevated sensitivity of polar ozone to EESC in the polar regions. The use of a semiempirical model such as SWIFT (Semiempirical Weighted Iterative Fit Technique) [*Rex et al*., 2013] in MAGICC for the polar regions could improve the simulation of the direct effects of GHGs on ozone Chapman chemistry and the indirect effects of GHGs on heterogeneous ozone chemistry via PSCs.

2.2. Statistical Modeling of wSCO

To account for the vertical dependence of RF on ozone in MAGICC, wSCO was trained similarly to equation (1) but with wSCO′ replacing SCO′. The weights (w) needed to calculate wSCO were obtained from the RF sensitivity function developed by *Lacis* [1990]

$$w_{i,j} = 0.334e^{-\frac{z_{i,j}}{3.6}} - 5.4\times10^{-5}\left(z_{i,j} - z_{\mathrm{th}}\right)^{1.4}\left(1 - 41e^{-\frac{z_{\mathrm{th}}}{7.5}}\right) \tag{3}$$

where z is the altitude in kilometers at latitude i and level j and z_{th} is the tropopause height. The location of the tropopause, which is also used to calculate the SCO, was determined using the WMO definition, i.e., the altitude at which the lapse rate falls below −2 K/km and stays below −2 K/km for at least 2 km.

2.3. Statistical Modeling of RF

A similar technique was used to determine the functional dependence of RF on wSCO. Because the radiative effect of stratospheric ozone varies with latitude, zonal mean wSCO′ for the combined polar regions (60°–90° N/S), the combined midlatitudes (30°–60°N/S) and the equatorial region (30°S–30°N) were used as predictors for global stratospheric ozone RF as

$$\mathrm{RF} = \sigma w\mathrm{SCO}'_{90°-60°} + \varphi w\mathrm{SCO}'_{60°-30°} + \omega w\mathrm{SCO}'_{30°-0°} + \epsilon \tag{4}$$

where the coefficients σ, φ, ω, and ϵ are derived by fitting equation (4) to wSCO′ calculated from the ozone database that was constructed in support of Coupled Model Intercomparison Project Phase 5 (CMIP5) simulations and corresponding stratospheric ozone RF [*Cionni et al*., 2011].

There are few archived CCM model simulations which provide latitudinally resolved ozone at monthly resolution and corresponding RF values that can be used for training a wSCO′ to RF regression model. There are also uncertainties in the RF used in the training, primarily due to outdated ozone absorption coefficients [*Cionni et al*., 2011]. These uncertainties propagate into the regression and therefore also the simulation of RF within MAGICC. Availability of a larger number of ozone and RF data sets from CCM simulations would make the training of the wSCO′ to RF regression model more robust.

To test whether the uncertainty in our regression-derived relationship between wSCO′ and ozone RF may affect our derived years of return of SCO to 1960 levels, a set of regression model coefficients, obtained by averaging the coefficients obtained for equatorial, midlatitude, and polar regions, was used to drive the wSCO′ to ozone RF. The years of return were shown to be largely insensitive to the wSCO′ to RF relationship encapsulated in the regression model.

2.4. An Interactive Stratosphere in MAGICC

The coefficients derived from equations (1), (2), and (4) are used in MAGGIC to calculate stratospheric ozone RF from SCO′ and wSCO′. The wSCO′ values are averaged over the three latitude zones 60°–90°S/N, 30°–60° S/N, and 30°S–30°N, and the resulting ozone RF is then calculated using equation (4). The ozone RF for the three latitude zones is summed to create an annual global stratospheric ozone RF. This global RF is partitioned into four regions, viz., northern hemisphere ocean and land and southern hemisphere ocean and land as required by the underlying MAGICC model, thereby coupling the MAGICC stratosphere to the climate system.

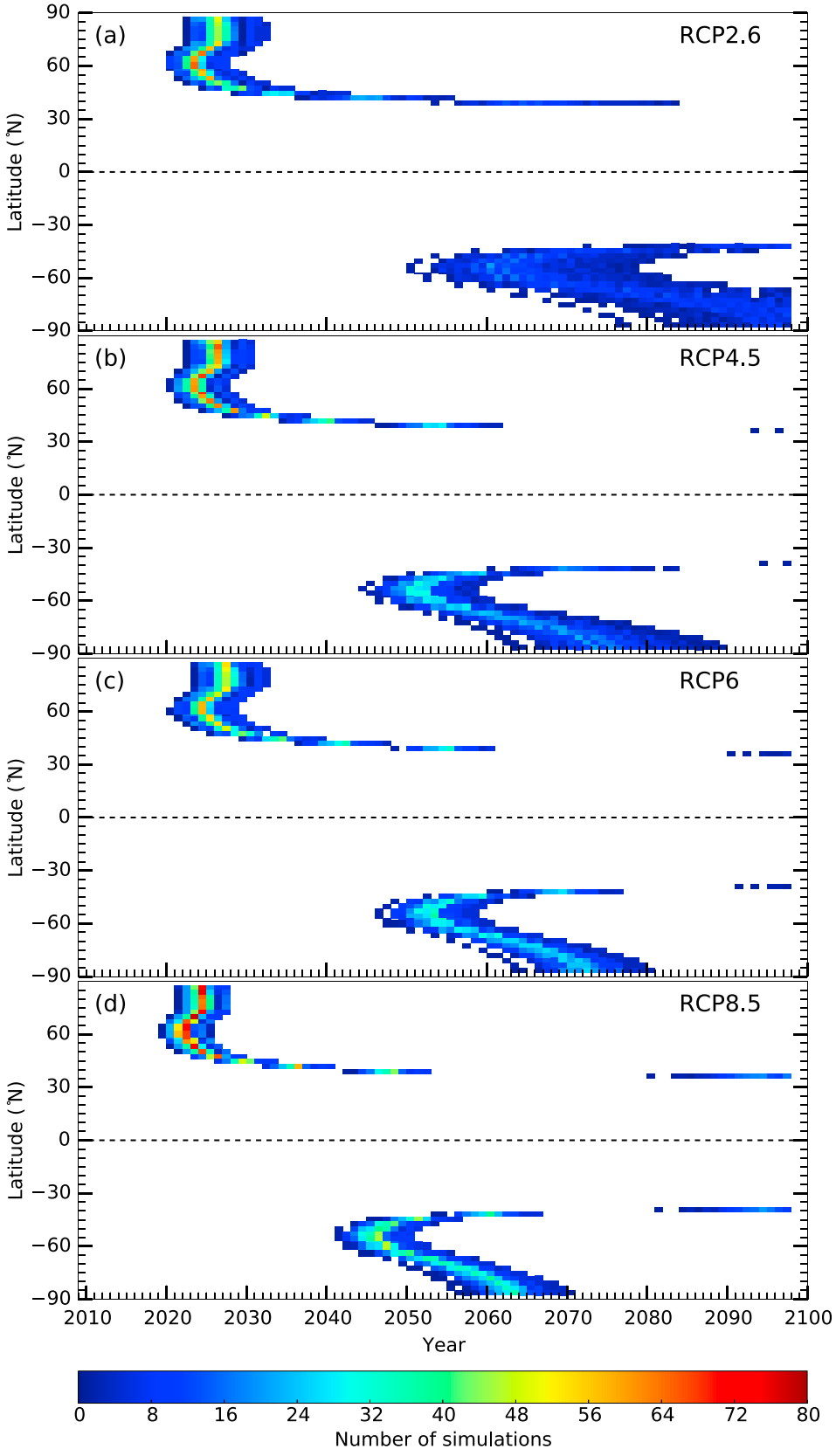

Figure 1. Probability of year of return of SCO to 1960 levels. The 180-member ensembles for 90°S to 90°N, simulated with MAGICC under four GHG emissions scenarios: (a) RCP2.6, (b) RCP4.5, (c) RCP6.0, and (d) RCP8.5.

Table 1. The Mean Years of Return of SCO to 1960 Levels [a]

	RCP2.6	RCP4.5	RCP6.0	RCP8.5
85°N	2025.2 ± 2.1	2024.9 ± 2.0	2026.1 ± 1.9	2023.0 ± 1.3
	[2022–2032]	[2022–2030]	[2023–2031]	[2021–2027]
60°N	2022.4 ± 1.9	2022.5 ± 1.6	2023.4 ± 1.9	2022.4 ± 1.3
	[2020–2028]	[2019–2027]	[2020–2028]	[2019–2025]
40°N	2066.1 ± 8.4	2052.3 ± 3.4	2053.3 ± 2.5	2046.4 ± 2.2
	[2053–2083]	[2046–2062]	[2048–2061]	[2042–2053]
40°S	[2072–]	2069.7 ± 4.8	2067.6 ± 3.0	2058.9 ± 2.5
		[2060–2084]	[2060–2077]	[2053–2067]
60°S	2067.9 ± 8.2	2053.2 ± 3.2	2054.2 ± 2.4	2047.2 ± 2.0
	[2052–2082]	[2046–2060]	[2047–2060]	[2042–2052]
85°S	[2076–]	2074.3 ± 6.0	2071.3 ± 3.1	2061.8 ± 2.5
		[2063–2089]	[2063–2080]	[2056–2070]

[a]The years of return of SCO are presented as the mean of the 180-member ensemble simulated under four different emissions scenarios. The uncertainties are expressed as $\pm 1\sigma$, and the range of years (maximum–minimum) of return to 1960 values are shown in brackets.

3. Results: Years of Return of Stratospheric Column Ozone to 1960 Levels

Tunings to 18 different AOGCMs and 10 different carbon cycle models used in the World Climate Research Programme's Coupled Model Intercomparison Project phase 3 (CMIP3) multimodel data set [*Meehl et al.*, 2007] and Coupled Carbon Cycle Climate Model Intercomparison Project [*Friedlingstein et al.*, 2006] are used to explore the effects of model structural uncertainty on the SCO projections and return dates. MAGICC is then run with an interactive stratosphere, for all 180 combinations of AOGCMs and carbon cycle model tunings, creating one ensemble for each of the four Representative Concentration Pathways (RCP) emissions scenarios, viz., RCP2.6, RCP4.5, RCP6, and RCP8.5 [*Moss et al.*, 2010], from 1960 to 2100. All simulations were run under the A1 ODS scenario [*WMO*, 2007].

The probabilities of the return dates of zonal mean SCO to 1960 levels for all RCP emissions scenarios are shown in Figure 1. The return to 1960 values is projected to occur earliest at midlatitudes, later in the polar regions and latest, if at all, in the tropics (Figure 1 and Table 1). The results presented here are consistent with previous studies [*Bekki et al.*, 2013; *Cionni et al.*, 2011; *Eyring et al.*, 2010b, 2013; *Garny et al.*, 2013] but now include robustly determined uncertainties in the dates of return.

At 60°N, under the RCP2.6 emissions scenario, SCO is expected to return to 1960 levels between 2020 and 2028, with an average year of return in 2022.4 ± 1.9 (ensemble mean $\pm 1\sigma$, as stated ranges hereafter) (Table 1) and with the most likely year of return (the mode of the ensemble) in 2023 (Figure 1). At 60°S, the mean year of return of SCO to 1960 levels is 2067.9 ± 8.2, ~45 years later, and with a larger uncertainty, compared to the return date at 60°N. Chemically induced changes in ozone [*Garny et al.*, 2013], as well as changes in ozone due to changes in the strength of the BDC [*WMO*, 2014; *Eyring et al.*, 2010a; *Butchart*, 2014], drive an earlier return of SCO to unperturbed levels in the Northern Hemisphere than in the Southern Hemisphere. An enhanced tropical upwelling, as a part of the BDC, is an important driver of reductions of ozone in the tropical lower stratosphere [*WMO*, 2014].

The largest spread in simulated years of return of SCO to 1960 levels is found at 40°N, 40°S and in the Antarctic. At 40°N, under RCP2.6, SCO is expected to return to 1960 levels in 2066.1 ± 8.4, with the 180-member ensemble ranging from 2053 to 2083 (Table 1). At 40°S, SCO is projected to return to unperturbed levels at the earliest in 2072, and some of the simulations suggest a return beyond 2100. With increasing GHG loading of the stratosphere, the ensemble spread in dates of return of extratropical latitude SCO to 1960 levels decrease. At 40°N the ensemble spread decreases from ±8.4 years when simulated under RCP2.6 to ±2.2 years under RCP8.5 (Table 1). Under RCP8.5, all simulations show a return of SCO to 1960 levels before the end of this century at 40°S, and the mean year of return is 2058.9 ± 2.5. At 40°N, under RCP8.5, SCO returns to 1960 levels 20 years earlier than under RCP2.6.

The minimum-maximum spread in simulated return years in the Arctic is 10 years under RCP2.6 and 6 years under RCP8.5. In the Antarctic, the range of return dates is more than 25 years (with values beyond 2100) under RCP2.6 and decreases to 14 years (with a $\pm 1\sigma$ of 2.5 years) under RCP8.5. Under RCP8.5, the return year

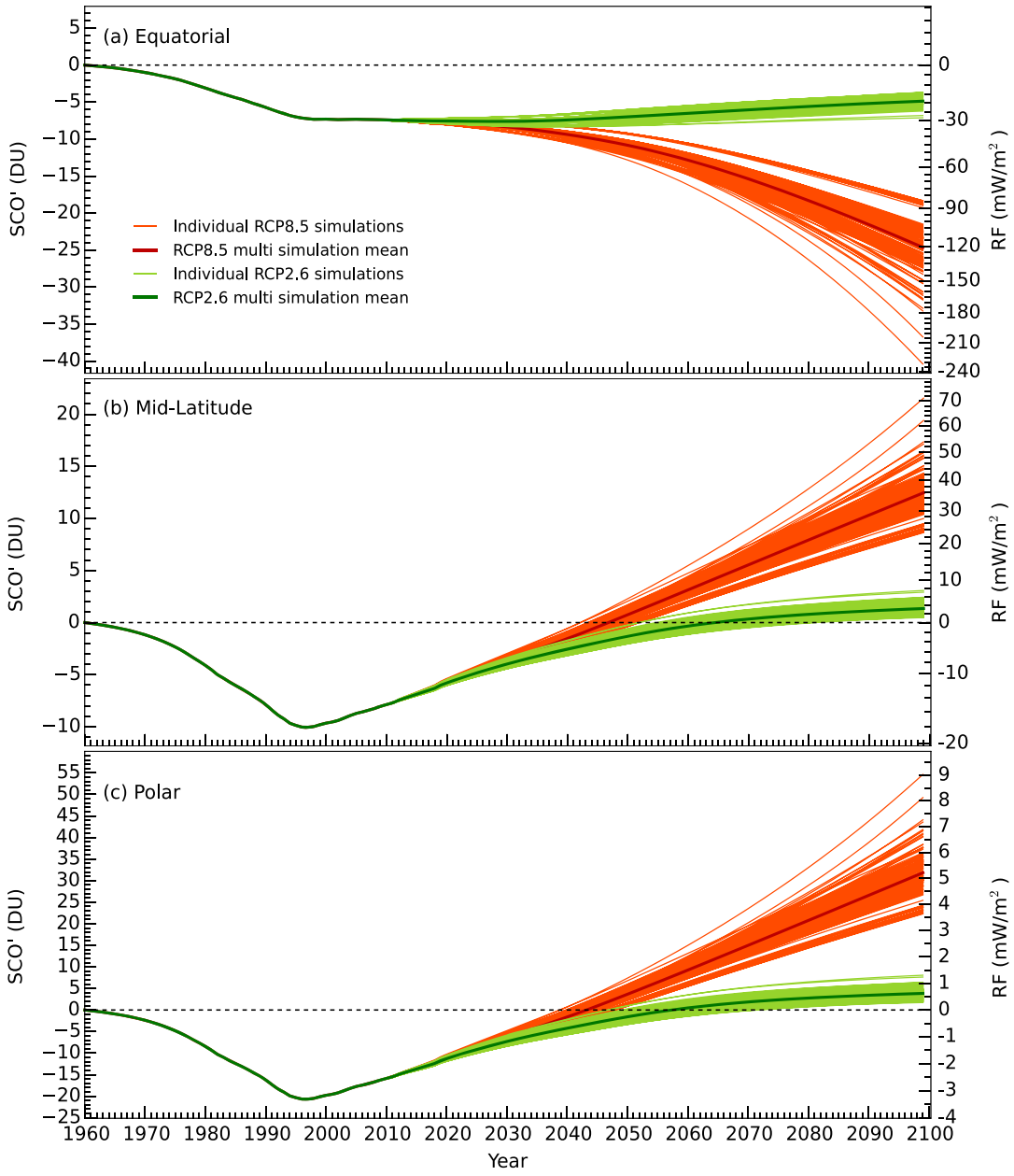

Figure 2. Ensembles of 180 simulations of zonal mean SCO′ corresponding approximate RF. The SCO anomalies are with respect to 1960 on the left-hand axis, while the corresponding approximate RF is shown on the right-hand axis, under RCP2.6 and RCP8.5, for three latitude zones: (a) Equatorial (30°S–30°N), (b) midlatitude (30°–60°S/N), and (c) polar (60°–90°S/N).

in the Arctic shifts earlier compared to RCP2.6, from 2025.2 to 2023.0. Until 2060, CO_2 emissions under RCP4.5 are larger than under RCP6.0 which results in SCO at some latitudes returning slightly earlier to 1960 levels for RCP4.5 compared to RCP6.0 (Figure 1 and Table 1).

3.1. Ensemble Simulations of SCO Anomalies

The differences in ensemble spreads of return years of SCO between different emissions scenarios can be understood by considering the evolution of SCO throughout the 21st century. SCO′ simulated under the RCP8.5 emissions scenario shows larger changes (decreases in tropics (30°S to 30°N) and increases in the midlatitudes (30° to 60°) and the polar regions (60° to 90°)) than under RCP2.6 and therefore crosses the zero anomaly line earlier and within a smaller range of years than under RCP2.6 (Figure 2). The simulations of SCO′

Table 2. Zonal Mean SCO′ and the Approximate Corresponding Mean RF Projected for the End of the Century (2100) [a]

	SCO′ (DU)		RF (mW/m^2)	
	RCP2.6	RCP8.5	RCP2.6	RCP8.5
Equatorial (0°–30°)	−4.9 ± 0.9 [−7.1 to −3.7]	−24.6 ± 3.4 [−40.4 to −18.3]	−20.4 ± 4.0 [−30.8 to −14.9]	−120.3 ± 19.7 [−232.6 to −80.1]
Midlatitudes (30°–60°)	1.3 ± 0.6 [0.5–3.1]	12.5 ± 1.9 [8.6–21.6]	3.2 ± 1.6 [0.9–7.9]	38.4 ± 7.3 [23.5–70.4]
Polar (60°–90°)	3.9 ± 1.5 [1.7–8.1]	31.8 ± 4.9 [22.3–54.6]	0. 6 ± 0.2 [0.3–1.3]	5.1 ± 1.0 [3.6–9.0]

[a]The SCO anomalies are with respect to 1960. The uncertainties are expressed as ±1σ, and the range of SCO′ and RF (minimum–maximum) are shown in brackets.

are averaged over the Southern and Northern Hemisphere 30° zones, since the RF from stratospheric ozone (right-hand axis in Figure 2, discussed below) in MAGICC is simulated over Southern and Northern Hemispheres zones combined.

Although tropical SCO is not projected to reach 1960 levels before the end of this century, the simulations under RCP2.6 indicate a slow increase from around 2030 onwards, consistent with previous studies [*Eyring et al*., 2010a, 2010b, 2013]. At the end of the century, the SCO ensemble mean under RCP2.6 is 4.9 Dobson units (DU) below 1960 levels, with an uncertainty of ± 0.9 DU (Table 2). Under the highest emissions scenario, SCO is likely to continue to decrease in the tropics due to a strengthening of the BDC, with the spread in simulations increasing to ± 3.4 DU. Under RCP8.5, while SCO′ decreases in the equatorial regions, it continues to increase in the middle and high latitudes, surpassing 1960 levels (Figure 2). At the end of the century, extratropical SCO is projected to reach levels well above those of 1960, especially under the RCP8.5 emissions scenario.

In the midlatitudes, under RCP2.6, the ensemble mean in 2100 is 1.3 DU above 1960 levels with an uncertainty of ± 0.6 DU, while under RCP8.5, the ensemble mean is more than 9 times larger (12.5 DU) with an uncertainty of ± 1.9 DU.

In the polar regions, the ensemble mean in 2100 under RCP8.5 is 8 times larger than the ensemble mean simulated under RCP2.6 and the uncertainty is more than 3 times larger (3.9 ± 1.5 DU *cf*. 31.8 ± 4.9 DU). At the end of the century the uncertainty in SCO′ simulated under RCP8.5 is more than twice as large in the polar regions than in the midlatitudes.

3.2. Ensemble Simulations of Stratospheric Ozone Radiative Forcing

By the end of the century, the ensemble mean ozone RF in the equatorial region simulated by MAGICC under RCP2.6 is −20.4 ± 4.0 mW/m^2 and under RCP8.5 −120.3 ± 19.7 mW/m^2 (right-hand axis of Figure 2 and Table 2). Noting the nonlinear scale on the right-hand axes in Figure 2, the spread in RF simulations, as for SCO, increases with increasing GHG loading. A negative RF contributes to a lowering of the surface temperature.

In the extratropics, the negative RF from stratospheric ozone maximizes in the mid-1990s due to substantial depletion of ozone by ODSs at that time (Figure 2). Thereafter, the negative RF from ozone decreases and is simulated to become positive in the middle of the 21st century.

In contrast to SCO, in the polar regions the ensemble mean RF, as well as the simulation spread, is smaller than in the midlatitudes, under both RCP2.6 and RCP8.5, due to the dependence on RF of the vertical distribution of ozone. By 2100, under RCP8.5, the 180-member ensemble mean RF in the midlatitudes is 38.4 ± 7.3 mW/m^2, more than 7 times larger than in the polar regions where the mean RF is 5.1 ± 1.0 mW/m^2. A stronger BDC enhances transport of ozone in the lower stratosphere from the tropics to the middle to high latitudes [*WMO*, 2014]. Since RF is affected mainly by ozone in the lower stratosphere, the largest change in RF is expected to be found where the largest change in lower stratospheric ozone takes place [*Lacis*, 1990]. Under RCP2.6, the ensemble mean RF is smaller than under RCP8.5 with a narrower uncertainty range: 3.2 ± 1.6 mW/m^2 in the midlatitudes and 0.6 ± 0.2 W/m^2 in the polar regions.

4. Discussion and Summary

The output from our 180-member ensemble simulation study shows that increasing GHG loading decreases the ensemble spread in projections of years of return of SCO to 1960 levels but increases the ensemble spread in SCO and corresponding RF simulations, due to increased spread in CO_2 (Figure S1). SCO′ as well as the spread in SCO′ increase with increasing GHG loading and decreasing EESC′. The influence of GHGs on SCO′ increases around the middle of this century, while the ozone-depleting effect of EESC becomes less important. To confirm the dominant effect from CO_2, MAGICC was run first with constant CO_2 and thereafter with constant EESC′. In the polar regions, for RCP8.5 simulations, the uncertainty in SCO′ at the end of the century decreases from ± 4.9 DU (Table 2) to ± 0.4 DU when CO_2 is kept constant, compared to a decrease to ± 4.7 DU when EESC is kept constant (Table S1). The same pattern is found in the equatorial region and the midlatitudes.

SCO is simulated to never reach 1960 levels when CO_2 is kept fixed and with changing EESC concentrations. Under RCP2.6, the differences between uncertainties in simulations when CO_2 is kept fixed and EESC′ is kept fixed are smaller compared to RCP8.5 simulations, since the total GHG loading is smaller, and therefore, the effect from EESC is greater (Table S1).

There is a clear relationship between the change in tropical upwelling, as part of the BDC, and the response of tropical ozone in the lower stratosphere, and CCMs show a wide range of responses of the BDC to a single emissions scenario [*Oman et al*., 2010]. The effect of the BDC on EESC′ in MAGICC is represented in terms of stratospheric lifetimes of halogenated gases, and the uncertainties in EESC′ ensemble simulations are largest at the end of the century, when the spread in simulated CO_2 concentrations and surface temperature are large (Figure S1). The BDC effect on the relationship between CO_2 (as a proxy for the stratospheric temperature), EESC′, and SCO′ is embedded in the simulations through the fitting of equation (1) to the EMAC model. To capture the full range of responses of the BDC to climate change across different CCMs, the method presented here could be used in the future to emulate a range of CCMs. For the present study, CO_2 is a proxy for temperature and climate-related effects in the settings of equation (1). In future work and further development of the SCM, other gases that affect stratospheric ozone concentrations such as methane and nitrogen oxide could be added to the regression (equation (1)). Thereby, contributions to uncertainties from compounds other than CO_2 and EESC could be estimated.

Since the output from our ensemble simulations are based on MAGIC emulations of different AOGCMs and carbon cycle models, the spreads in simulations may be different compared to what would be generated by an ensemble of 180 CCM simulations. Selected sets of key parameters are used to force MAGICC to emulate the behavior of any one of 18 different AOGCMS and any one of 10 different carbon cycle models; parameter sets optimize the ability of MAGICC to simulate global-mean temperatures and ocean heat uptake [*Meinshausen et al*., 2011a, 2011b]. The different sets of parameters, captured in MAGICC, determine the spread in our ensemble of SCO projections using MAGICC. It is not possible to include the full range of parameter possibilities (i.e., as included in each one of the AOGCMs and carbon cycle models) in the tuning of MAGICC. This limits our ability to capture the full range of uncertainty [*Meinshausen et al*., 2011a, 2011b]. Furthermore, in MAGICC common forcing agents, for example, forcing from CO_2, tropospheric ozone, and direct black carbon, are averaged over all emulated AOGCMs, and therefore, model spread due to differences in the forcing agents is not accounted for, which further narrows the spread of simulations [*Meinshausen et al*., 2011a, 2011b] and therefore also in our MAGICC simulations.

Previous multimodel studies of years of return of stratospheric ozone to unperturbed levels include simulations either from groups of CCMs that are run under a single GHG emissions scenario [*Eyring et al*., 2007, 2010a] or from only a few CCM simulations run under a set of emissions scenarios [*Eyring et al*., 2010b, 2013]. Agreement of the mean behavior of our ensemble of simulations with the results of these earlier studies provides confidence in the overall behavior of our simulations. Since our study is the first to provide a full probability density function (PDF) of projections of SCO, it is not possible to validate our PDFs against these earlier studies.

Acknowledgments
We would like to thank the New Zealand Antarctic Research Institute for funding this project. We would also like to thank Stefanie Meul for EMAC output data, Irene Cionni for contributing the ozone data from the CMIP5 ozone database, David Stevenson for radiative forcing data, and Alexandru Rap for helpful discussions regarding radiative forcing. MAGICC can be downloaded from the following website: http://www.magicc.org/.

References

Bekki, S., A. Rap, V. Poulain, S. Dhomse, M. Marchand, F. Lefevre, P. M. Forster, S. Szopa, and M. P. Chipperfield (2013), Climate impact of stratospheric ozone recovery, *Geophys. Res. Let.*, *40*(11), 2796–2800, doi:10.1002/grl50358.
Butchart, N. (2014), The Brewer-Dobson circulation, *Rev. Geophys.*, *52*, 157–184, doi:10.1002/2013RG000448.

Charlton-Perez, A. J., et al. (2010), The potential to narrow uncertainty in projections of stratospheric ozone over the 21st century, *Atmos. Chem. Phys.*, *10*(19), 9473–9486, doi:10.5194/acp-10-9473-2010.
Cionni, I., V. Eyring, J. F. Lamarque, W. J. Randel, D. S. Stevenson, F. Wu, G. E. Bodeker, T. G. Shepherd, D. T. Shindell, and D. W. Waugh (2011), Ozone database in support of CMIP5 simulations: Results and corresponding radiative forcing, *Atmos. Chem. Phys.*, *11*(21), 11,267–11,292, doi:10.5194/acp-11-11267-2011.
Daniel, J. S., S. Solomon, R. W. Portmann, and R. R. Garcia (1999), Stratospheric ozone destruction: The importance of bromine relative to chlorine, *J. Geophys. Res.*, *104*, 23,871–23,880, doi:10.1029/1999JD900381.
Eyring, V., et al. (2007), Multimodel projections of stratospheric ozone in the 21st century, *J. Geophys. Res.*, *112*, D16303, doi:10.1029/2006JD008332.
Eyring, V., et al. (2010a), Multi-model assessment of stratospheric ozone return dates and ozone recovery in CCMVal-2 models, *Atmos. Chem. Phys.*, *10*(19), 9451–9472, doi:10.5194/acp-10-9451-2010.
Eyring, V., et al. (2010b), Sensitivity of 21st century stratospheric ozone to greenhouse gas scenarios, *Geophys. Res. Lett.*, *37*, L16807, doi:10.1029/2010GL044443.
Eyring, V., et al. (2013), Long-term ozone changes and associated climate impacts in CMIP5 simulations, *J. Geophys. Res. Atmos.*, *118*, 5029–5060, doi:10.1002/jgrd.50316.
Forster, P. M., and K. P. Shine (1997), Radiative forcing and temperature trends from stratospheric ozone changes, *J. Geophys. Res.*, *102*, 10,841–10,855.
Friedlingstein, P., et al. (2006), Climate-carbon cycle feedback analysis: Results from the C4MIP model intercomparison, *J. Clim.*, *19*, 3337–3353, doi:10.1175/JCLI3800.1.
Garny, H., G. E. Bodeker, D. Smale, M. Dameris, and V. Grewe (2013), Drivers of hemispheric differences in return dates of mid-latitude stratospheric ozone to historical levels, *Atmos. Chem. Phys.*, *13*(15), 7279–7300, doi:10.5194/acp-13-7279-2013.
Gauss, M., et al. (2006), Radiative forcing since preindustrial times due to ozone change in the troposphere and the lower stratosphere, *Atmos. Chem. Phys.*, *6*(3), 575–599, doi:10.5194/acp-6-575-2006.
Hamill, P., O. B. Toon, and R. P. Turco (1986), Characteristics of polar stratospheric clouds during the formation of the Antarctic ozone hole, *Geophys. Res. Lett.*, *13*, 1288–1291, doi:10.1029/GL013i012p01288.
Huck, P. E., G. E. Bodeker, S. Kremser, A. J. McDonald, M. Rex, and H. Struthers (2013), Semi-empirical models for chlorine activation and ozone depletion in the Antarctic stratosphere: Proof of concept, *Atmos. Chem. Phys.*, *13*(6), 3237–3243, doi:10.5194/acp-13-3237-2013.
Jöckel, P., et al. (2006), The atmospheric chemistry general circulation model ECHAM5/MESSy1: Consistent simulation of ozone from the surface to the mesosphere, *Atmos. Chem. Phys.*, *6*(4), 5067–5104, doi:10.5194/acpd-6-6957-2006.
Jonsson, A. I., J. de Grandpré, V. I. Fomichev, J. C. McConnell, and S. R. Beagley (2004), Doubled CO_2-induced cooling in the middle troposphere: Photochemical analysis of the ozone radiative feedback, *J. Geophys. Res.*, *109*, D24103, doi:10.1029/2004JD005093.
Kremser, S., G. E. Bodeker, and J. Lewis (2014), Methodological aspects of a pattern-scaling approach to produce global fields of monthly means of daily maximum and minimum temperature, *Geosci. Model Dev.*, *7*, 249–266, doi:10.5194/gmd-7-249-2014.
Lacis, A. A. (1990), Radiative forcing of climate by changes in the vertical distribution of ozone, *J. Geophys. Res.*, *95*, 9971–9981, doi:10.1029/JD095iD07p09971.
Meehl, G. A., C. Covey, K. E. Taylor, T. Delworth, R. J. Stouffer, M. Latif, B. McAvaney, and J. F. B. Mitchell (2007), The WCRP CMIP3 multi-model dataset: A new era in climate change research, *Bull. Am. Meteorol. Soc.*, *88*, 1383–1394, doi:10.1175/BAMS-88-9-1383.
Meinshausen, M., S. C. B. Raper, and T. M. L. Wigley (2011a), Emulating coupled atmosphere-ocean and carbon cycle models with a simpler model, MAGICC6—Part 1: Model description and calibration, *Atmos. Chem. Phys.*, *11*(4), 1417–1456, doi:10.5194/acp-11-1417-2011.
Meinshausen, M., S. C. B. Raper, and T. M. L. Wigley (2011b), Emulating coupled atmosphere-ocean and carbon cycle models with a simpler model, MAGICC6—Part 2: Applications, *Atmos. Chem. Phys.*, *11*(4), 1457–1471, doi:10.5194/acp-11-1457-2011.
Mitchell, T. D. (2003), Pattern scaling, an examination of the accuracy of the technique for describing future climates, *Clim. Change*, *60*, 217–242.
Moss, R. H., et al. (2010), The next generation of scenarios for climate change research and assessment, *Nature*, *463*, 747–756, doi:10.1038/nature08823.
Newman, P. A., J. S. Daniel, D. W. Waugh, and E. R. Nash (2007), A new formulation of equivalent effective stratospheric chlorine (EESC), *Atmos. Chem. Phys.*, *7*, 4537–4552.
Nowack, P., N. L. Abraham, A. C. Maycock, P. Braesicke, J. M. Gregory, M. M. Joshi, A. Osprey, and J. A. Pyle (2015), A large ozone-circulation feedback and its implications for global warming assessments, *Nature Clim. Change*, *5*, 41–45, doi:10.1038/nclimate2451.
Oman, L. D., et al. (2010), Multimodel assessment of the factors driving stratospheric ozone evolution over the 21st century, *J. Geophys. Res.*, *115*, D24306, doi:10.1029/2010JD014362.
Randall, D. A., et al. (2007), Climate models and their evaluation, in *Climate Change 2007: The Physical Science Basis. Contribution of Working Group I to the Fourth Assessment Report of the Intergovernmental Panel on Climate Change*, edited by S. D. Solomon et al., pp. 643–645, Cambridge Univ. Press, Cambridge, U. K., and New York.
Rex, M., S. Kremser, P. Huck, G. Bodeker, I. Wohltmann, M. L. Santee, and P. Bernath (2013), Technical note: SWIFT—A fast semi-empirical model for polar stratospheric ozone loss, *Atmos. Chem. Phys.*, *13*(12), 31,607–31,634, doi:10.5194/acpd-13-31607-2013.
Shepherd, T. G., and A. I. Jonsson (2008), On the attribution of stratospheric ozone and temperature changes to changes in ozone-depleting substances and well-mixed greenhouse gases, *Atmos. Chem. Phys.*, *8*(5), 1435–1444, doi:10.5194/acp-8-1435-2008.
World Meteorological Organization (WMO) (2007), Scientific assessment of ozone depletion: 2006, Global Ozone Research and Monitoring Project - Report No. 50, Geneva, Switzerland.
World Meteorological Organization (WMO) (2014), Scientific assessment of ozone depletion: 2014, Global Ozone Research and Monitoring Project-Report No. 56, Geneva, Switzerland.